Activation of visible up-conversion luminescence in transparent and conducting ZnO:Er:Yb films by laser annealing

M. Lluscà[a,*], J. López-Vidrier[b], S. Lauzurica[c], M. I. Sánchez-Aniorte[c], A. Antony[a,d], C. Molpeceres[c], S. Hernández[b], B. Garrido[b] and J. Bertomeu[a]

[a] *Department of Applied Physics and Optics, Universitat de Barcelona, Barcelona 08028, Spain*

[b] *Department of Electronics, Universitat de Barcelona, Barcelona 08028, Spain*

[c] *Centro Laser, Universidad Politécnica de Madrid, Madrid 28031, Spain*

[d] *Indian Institute of Technology Bombay, Mumbai 400076, India*

*E-mail: marta.llusca@ub.edu; Tel: +34 9340 39223

1. Introduction

Most thin film solar cells are not able to absorb photons with energy lower than its band gap and this is very much applicable for photons in the near infrared wavelength. One way to enhance low energy photon absorption could be to convert these photons into higher energy ones by using rare earth (RE) ions such as Er and Yb. Rare earth materials have been widely studied due to their photoluminescence properties, which occur as a result of their intra 4*f*-4*f* shell transitions [1]. In particular, Er and Yb co-doped systems [2-4] have the capability to cooperate together to convert infrared radiation into visible light because of their energy levels matching for $\lambda = 980$ nm [5]. Yb species act as the absorber ions due to their higher absorption coefficient, thus absorbing the incoming low-energy photons (980 nm), whereas Er species act as the emitter ions, releasing higher-energy photons (550 nm, 660 nm, etc.) (see Fig. 1). In this work, ZnO has been chosen as the host matrix for Er and Yb ions with the intention to create a transparent and conducting up-converting material that will function as the transparent conducting oxide (TCO) back contact as well as to, exploit the up-conversion mechanism to enhance the efficiency of the solar cells.

The substitutional doping of Er ions in to the ZnO matrix forming a planar ErO_4 conformation results in a non-optically active state, whereas Er ions fully surrounded by oxygen atoms in a pseudo-octahedron structure with a C_{4v} symmetry (ErO_6 clusters) are optically active centers that allow the 4*f*-4*f* transitions to occur [6]. A thermal annealing is necessary to optically activate the Er ions by changing the Er local structure into the form of ErO_6 clusters, either inside the ZnO matrix or at their grain boundaries [7,8].

In this study, ZnO:Er:Yb films were deposited by radio-frequency (RF) magnetron sputtering and optical activation of Er ions was achieved by annealing the samples by three different methods i) 800°C in air atmosphere, ii) 800°C in vacuum, and iii) laser annealing at ambient temperature using a 532-nm continuous wave (CW) laser radiation. The objective of these annealing processes was to optically activate Er ions to produce up-conversion while preserving the transparency and conductivity of the films. The composition of the films, the crystalline structure, electrical and optical properties of the RE-doped ZnO films were studied before and after the different annealing treatments and the results are presented in the following sections.

2. Experimental details

ZnO:Er:Yb thin film was deposited onto a 10×10 cm^2 Corning 1737F glass substrate by means of an RF magnetron sputtering using ATC-ORION 8 HV from AJA International Inc. The doping of Er and Yb was achieved by placing one Er_2O_3 pellet and three Yb_2O_3 pellets on the erosion area of the ZnO target. The ZnO target was 99.995% pure and had a diameter of 3 inches. The pellets (13 mm diameter) were made by pressing Er_2O_3 and Yb_2O_3 powders of 99.99% purity with a Specac Hydraulic Press, and the as-prepared pellets were annealed in O_2 flow at 800°C for 4 hours in a quartz tubular furnace. The film was deposited with an RF power of 120 W at 0.4 Pa argon

pressure. The target to substrate distance was 14 cm and there was no intentional heating of the substrate during the deposition. The film thickness was 800 nm.

In order to analyze the influence of the annealing methods, 6 identical pieces of 1×1 cm^2 area were cut from the as-deposited ZnO:Er:Yb film and underwent different annealing treatments. Among the six samples, one piece was kept without any annealing treatment (AS DEP) for comparison purposes; the second sample was annealed in air atmosphere (AIR) at 800°C during 1 hour in a conventional quartz tubular furnace; the third piece was annealed at 800ºC in vacuum (VAC) of 2.1×10^{-4} Pa for 1 hour; and the three remaining samples were subjected to LASER annealing with a CW, diode-pumped and frequency-doubled Nd:YVO_4 laser (Spectra-Physics Millennia Pro), yielding an emission wavelength of 532 nm. The beam spot on the sample was 29 μm in diameter. The laser annealing process was performed in air atmosphere by scanning 10×10 mm^2 areas with parallel lines without any gap between them. The scanning speed used was 400 mm/s and the three irradiation conditions used for the laser annealing were; **LAS1**: P=0.05 W, peak fluence=0.37 J/cm^2, **LAS2:** P=0.1 W, peak fluence=0.74 J/cm^2 and **LAS3:** P=0.2 W, peak fluence=1.48 J/cm^2. The composition, structure, electrical and optical properties of all the samples were analyzed and compared with that of the as-deposited one.

X-ray photoelectron spectroscopy (XPS) was used to determine the elemental composition using a PHI 5500 Multitechnique system from Physical Electronics. A pre-sputtering of the sample surfaces was carried out for 3 min using argon gas before recording the XPS spectra. The composition of the films was estimated from the integrated peak areas of the spectra. The crystallinity of the ZnO:Er:Yb films was analyzed using X-ray diffraction (XRD) by a PANalytical X'Pert PRO MPD Alpha1 diffractometer set under Bragg-Brentano geometry (θ-2θ scans).

To evaluate the feasibility of the films as a transparent and conducting oxide, the transmittance (*T*) and the sheet resistance (*Rs*) of all the samples were measured. The *T* was recorded using a Perkin Elmer Lambda 950 spectrophotometer with a 150-mm integrating sphere. The integrated *T* values were calculated within the visible range of wavelength (400-800 nm) of light. The resistivity (ρ) of the films was calculated from the sheet resistance *Rs* measured using a Jandel RM3 four-point probe station.

Conventional photoluminescence (PL) spectra were acquired using a Horiba Jobin-Yvon LabRam spectrometer coupled to a high-sensitive CCD detector. The 325-nm line of a He-Cd laser (Kimmon IK Series) was employed to excite the sample through a UV objective of 15× magnification and at a long-working distance (NUV-LWD). The emission was collected in backscattering geometry, using the same optics. The sample was kept at liquid nitrogen temperature (−196°C) using a Linkam cryostat. All acquired spectra were corrected for the system response.

Up-conversion PL (UC-PL) measurements were performed using an EKSPLA PG122 optical parametric oscillator (OPO) with an output range of 420-2300 nm, pumped by the third harmonic of a Brilliant 5-ns-pulsed Nd:YAG laser (355 nm). In particular, the OPO output at 980 nm was selected, with the aim of exciting the $^4I_{11/2}$ and $^2F_{5/2}$ levels of Er^{3+} and Yb^{3+} ions, respectively. The resulting visible spectra were acquired by a GaAs photomultiplier tube coupled to a monochromator, using a spectral resolution below 1 nm.

3. Results and discussion

XPS analysis revealed that the composition of the films in terms of Er and Yb atomic contents remained invariant at 0.5 at.% and 2.5 at.%, respectively, regardless of

the annealing method. Fig. 2 presents the XRD patterns of the as-deposited and the annealed ZnO:Er:Yb samples.

The ZnO:Er:Yb films showed the strong *c*-axis orientation of (002) plane and its second order reflection (004) of the hexagonal ZnO wurtzite structure. In the case of the as-deposited ZnO:Er:Yb film, no Er_2O_3 or Yb_2O_3 related phases were observed, suggesting that the RE ions are either substitutionally replacing Zn in the ZnO lattice or segregated to the grain boundaries. The annealing process, however, induced the appearance of different phases within the XRD patterns. The peak at $2\theta = 29.62°$ that appeared in both air and vacuum annealed films corresponds to the (222) reflection of Yb_2O_3 cubic structure [9]. The Er_2O_3 related peaks were not shown by any of the films, probably due to the rather small amount of Er content in the films (below the detection limit of the instrument). In the laser annealed samples, only the peaks related to ZnO wurtzite reflections were observed. Assuming hexagonal structure the lattice parameter value *c* was calculated from the (002) peaks, and the values are tabulated in Table 1.

The lattice parameter calculated for the as-deposited film is slightly larger than that of undoped poly crystalline ZnO (c=5.21 Å) [10], indicating a higher compressive stress, caused mainly by the ion bombardment during the sputtering process [11]. The thermal annealing in air and in vacuum contributed to the lattice relaxation, and the *c* parameter values became closer to that of undoped ZnO. A slight tensile stress was also observed and this was due to the mismatch between the thermal energy coefficients of the Corning 1737F glass substrate and the film, when the samples were cooled down to room temperature after annealing [12]. In the case of laser annealed samples, the (002) peak was barely shifted which implies that the laser fluence employed for the annealings was almost not affecting the film stress.

Fig. 3 shows the transmission spectra of the thermal- and laser-annealed samples, compared to the as-deposited one. The inset table presents the integrated *T* values within the visible range of wavelength of light (400–800 nm). The samples were found to be very transparent and showed transmittance beyond 84% when the samples were thermally annealed, due to the enhancement of the stoichiometry rather than the crystallinity of the films, as reported by Ahan *et al.* in [13].

The electrical properties of bulk ZnO are, as in any other solid material, tightly related to its crystalline structure. In particular, the conduction mechanism of ZnO films is mainly due to the electrons supplied from the donor sites associated with oxygen vacancies and zinc interstitials. The as-deposited ZnO films doped with metallic Er and Yb species showed higher electrical conductivity than pure ZnO films due to the contribution of Er^{3+} and Yb^{3+} ions incorporated at the substitutional sites of Zn^{2+} ions, as well as the presence of the aforementioned oxygen vacancies and zinc interstitials [14]. The resistivity values of the as-deposited film and of the samples subjected to different annealing methods were calculated from the electrical sheet resistance measurements. The as-deposited ZnO:Er:Yb showed a resistivity of 5×10^{-2} Ω·cm which increased to 1×10^{4} Ω·cm upon thermal annealing in air. This increase in resistivity can be ascribed to either the decrease of oxygen vacancies or to the chemisorption of O_2 that might have been trapped at the grain boundaries during air annealing. Both cases would reduce the density of donor sites and/or the RE interstitial atoms, resulting in the decrease of the carrier concentration and a rise of the potential barrier, which would consequently reduce the mobility of the films [14-16]. The vacuum annealing of the films resulted in a resistivity of 4×10^{-1} Ω·cm, which is only one order of magnitude higher than the as-deposited ones. In the case of the laser-annealed films the conductivity did not change, irrespective of the laser power, which implies that air

molecules did not take part in the local structure modification carried out by the surface-concentrated radiation annealing.

The effect of the different annealing treatments on the luminescence properties of the ZnO:Er:Yb films was also investigated by means of PL. The films were excited using 325 nm, and the temperature of the samples was kept constant at −196°C during the measurements, in order to minimize the defects-related emission and decays via non-radiative paths within the material. It should be mentioned that the different PL spectra were obtained under exactly the same conditions, and hence a direct comparison between the recorded intensities is perfectly feasible and reliable. Fig. 4 shows the PL emission spectra of each of these samples acquired in the range 330–850 nm, whereas the inset presents their emission around λ=980 nm indicating the effect of each annealing treatment on the Er^{3+} and Yb^{3+} common electronic transition. The first observation is that the non-treated ZnO:Er:Yb sample did not show any PL emission, implying the need of a post-deposition annealing treatment to optically activate the matrix. The air- and vacuum-annealed samples exhibit the maximum emission intensity along the whole spectral range (350–1020 nm).

The UV emission peak for the air- and vacuum-annealed samples at 372–375 nm corresponds to the band-to-band excitonic recombination, and the broad band centered around 660 nm is attributed to deep intra-band gap energy states generated by defects within the ZnO matrix [17]. The shape and position of this visible band depend on the defect state populations. In the case of green emission, it is mostly associated with oxygen vacancies [18]. However, some authors assign it to zinc interstitial positions [19]. When the emission is yellow, orange and red, like in our case, it is mainly related to an excess of oxygen [18, 20], oxygen interstitials [21-23] or zinc vacancies [20]. In our measurements we observe that the ratio of the intensities for visible defects-related

band in respect to the UV band-to-band radiative recombination is much larger for the air annealed sample, which indicates a significant incorporation of oxygen and, thus, a reduction of oxygen vacancies. Since the Er and Yb doping concentration is the same for air and vacuum annealed samples, oxygen and nitrogen incorporation during the air-annealing may be playing an important role in their photoluminescence properties.

The enhancement in the UV emission is related to a higher stoichiometry of the films, and can be improved by oxygen incorporation through a post-deposition annealing process [15, 24, 25]. The PL emission observed from the laser-annealed samples, much lower in intensity than the former ones, suggests that the film stoichiometry does not vary with respect to the as-deposited film. This observation agrees with the XRD results, where almost no variation of the lattice parameter occurred with laser annealing (see Table 1). Therefore, we can conclude that laser annealing prevents the uncontrolled insertion of oxygen within the ZnO matrix, probably due to the very short exposure times for the laser heating in each point (some tens of milliseconds).

Apart from the matrix (ZnO)-related PL, Fig. 4 also shows a peak at 750 nm for the air annealed sample, attributed to the second order of the excitonic recombination-related emission. And the emission around 660 nm corresponds to an Er^{3+} relaxation ought to the $^4F_{9/2} \rightarrow {}^4I_{15/2}$ transition (see Fig. 1). The near infrared part of the spectra (inset of Fig. 4) presents an emission peak, centered at 980 nm, corresponding to either the Er^{3+} $^4I_{11/2} \rightarrow {}^4I_{15/2}$ or Yb^{3+} $^2F_{5/2} \rightarrow {}^2F_{7/2}$ electronic transitions (or to a combination of both). The clear observation of this intra 4f-shell transition is a strong evidence for the optical activation of the RE ions introduced inside the ZnO matrix. To directly excite the RE ions and induce inter-level transitions, the incident photons need to have an energy resonant with one of their electronic levels. Therefore, the 325-nm laser

excitation should not be able to produce such effects. Nevertheless, a possible energy transfer can take place from the host matrix to the integrated ions, which is translated into their excitation [5, 26]. As observed in Fig. 4, this energy transfer occurs in all annealed samples, where the ZnO matrix is optically active. Er^{3+} and Yb^{3+} ions might occupy optically active sites either in the host matrix lattice or in the grain boundaries.

In the case of laser annealing, the spectra display a low PL efficiency at 980 nm with respect to other annealing treatments. This could be due to the lack of incorporation of oxygen atoms into the lattice during laser annealing, which strongly decreases the ZnO excitation, quenches the PL emission, and consequently the energy transfer to RE ions. In addition, when locally studying the different laser annealing processes, LAS3 presents a higher PL emission at 980 nm than LAS1 and LAS2, the latter ones exhibiting a nearly flat spectrum. The employed laser power is notably affecting the local arrangement of RE ions within the ZnO lattice, allowing their optical activation. In particular, a higher laser power seems to improve the local environment of Er^{3+} and Yb^{3+} ions, which is translated into more stable levels within the ZnO band gap. Contrary to what was expected, LAS2 shows lower emission at 980 nm than LAS1, but the difference is almost negligible and might be related to the non-uniform film or to the manually chosen focus point during the PL measurement.

To further understand the annealing effect on the RE ions incorporated inside the host matrix, room-temperature up-conversion experiments were performed. Provided that PL emission was observed at 980 nm (see inset of Fig. 4) indicating the activation of Er^{3+} transitions $^4I_{11/2} \rightarrow {}^4I_{15/2}$ and Yb^{3+} $^2F_{5/2} \rightarrow {}^2F_{7/2}$, the samples were excited at this particular wavelength by means of a ns-pulsed Nd:YAG laser coupled to an OPO. The acquired UC-PL spectra (under 980-nm laser excitation) are displayed in Fig. 5.

No emission was observed from the untreated sample which is in good accordance with the PL results, and may be due to the fact that the surrounding of RE is not adequate to realize up-conversion, and consequently a post-deposition annealing process is necessary. In the case of the annealed samples, the emission intensity of the air and vacuum treatments is in agreement with the one observed in conventional PL spectra: the presence of oxygen enhances RE-related emission/absorption, probably by propitiating the generation of ErO_6 regions [6]. The laser annealed samples show, a very poor up-conversion emission for LAS1 and LAS2, whereas an intense emission is displayed by LAS3, owing to the higher laser power employed. This latter fact establishes a minimum laser power requisite for the proper ordering of the RE atomic environment. In Er-Yb systems, the most probable up-conversion mechanism concerns the Yb^{3+} $^2F_{7/2} \rightarrow {}^2F_{5/2}$ transition, whose emission populates the $^4I_{11/2}$ and $^4F_{7/2}$ excited states of the Er^{3+} ions, via multiple photon absorption. After relaxation (probably via non-radiative phonon-related processes), $^2H_{11/2}$,$^4S_{3/2}$, and $^4F_{9/2}$ states become populated, whose radiative decay originates visible emissions at 520, 550 and 660 nm, respectively. The fact that we are only observing emission at 660 nm supports a different process. In this new frame, the excitation of the $^4I_{11/2}$ state can be followed by a non-radiative decay to the immediately-lower energy ($^4I_{13/2}$) level, and the additional energy transfer from Yb^{3+} causes an excitation to the $^4F_{9/2}$ state [27, 28], which is responsible for the up-conversion emission at 660-nm. Fig. 1 summarizes both possible processes leading to up-conversion within the system under study. The integration of RE ions within the ZnO matrix has been proved to generate optically active centers able to provide high-energy photons out of the absorbed low-energy ones by means of the up-conversion process. The results shown here establish laser annealing as an alternative to conventional thermal annealing (under air or in vacuum) to obtain

comparable up-conversion properties with an added advantage of preserving the film conductivity and transparency. Besides, it has been shown that a minimum laser power is required for the correct structural modification of the RE environment, which is essential for the good optical performance of Er^{3+} and Yb^{3+} ions to produce up-conversion.

4. Conclusions

800-nm-thick ZnO:Er:Yb films deposited on Corning 1737F glass by RF magnetron sputtering have been annealed under different conditions in order to create a transparent and conducting up-converter to be used as the TCO, e. g. as the back reflector of an a-Si solar cell. Air annealing, vacuum annealing, and laser annealing at three different laser powers have been carried out, and the properties of these treated films have been compared to those of the as-deposited film. All films showed typical ZnO wurtzite structure with (002) preferential orientation, and Yb oxide was only seen for the vacuum- and air-annealed ones. The as-deposited film presented a resistivity of 5×10^{-2} Ω·cm which increased to 4×10^{-1} Ω·cm for the vacuum annealing, and to 1×10^{4} Ω·cm in the case of thermal annealing in air. The resistivity remained invariant with the laser treatment and films remained conducting. In all cases the annealed samples presented an integrated transmittance within the visible range (400-800 nm) higher than 78%. Visible up-conversion was achieved in all annealed films, the most efficient being the film annealed in air, followed by the laser annealing at 1.48 J/cm^2. The overall results suggest that laser annealing is an alternative to more conventional high temperature annealing processes, presenting a similar transparency with an added advantage of preserving the conductivity of the as-deposited film as well. Therefore, it has been demonstrated that it is possible to create an adequate Er environment that

allows its 4*f*-4*f* transitions in a film that is conductive and transparent enough to be used as a TCO for various applications. Still, deeper research is to be done to study the feasibility of incorporating ZnO:Er:Yb thin film as the TCO to be used in solar cells: in particular, a better equilibrium has to be reached between the up-conversion mechanism and the electrical properties of the films.

Acknowledgments

This work was supported by the Spanish Ministerio de Economía y Competitividad and the European Regional Development Fund through the projects AMIC (ENE2010-21384-C04-03), HELLO (ENE2013-48629-C4-2/3-R), LEOMIS (TEC2012-38540-C02-01) and INNDISOL (IPT-420000-2010-6).

References

[1] B.M. van der Ende, L. Aarts, and A. Meijerink, Lanthanide ions as spectral converters for solar cells, Phys. Chem. Chem. Phys. 11 (2009) 11081–11095.

[2] J.F. Philipps, T. Töpfer, H. Ebendorff-Heidepriem, D. Ehrt, and R. Sauerbrey, Spectroscopic and lasing properties of Er^{3+}:Yb^{3+}-doped fluoride phosphate glasses, Appl. Phys. B 72 (2001) 399–405.

[3] A.S. Oliveira, M.T. de Araujo, A.S. Gouveia-Neto, J.A. Medeiros Neto, A.S.B. Sombra, and Y. Messaddeq, Frequency upconversion in Er^{3+}/Yb^{3+}-codoped chalcogenide glass, Appl. Phys. Lett. 72 (1998) 753–755.

[4] M. Wang, C. Mi, W. Wang, C. Liu, Y. Wu, Z. Xu, B. Mao, and S. Xu, Immunolabeling and NIR-excited fluorescent imaging of HeLa cells by using $NaYF_4$:Yb,Er upconversion nanoparticles, ACS Nano 3 (2009) 1580–1586.

[5] M. Lluscà, J. López-Vidrier, A. Antony, S. Hernández, B. Garrido, J. Bertomeu, Up-conversion effect of Er- and Yb-doped ZnO thin films, Thin Solid Films, 562 (2014) 456–461.

[6] M. Ishii, S. Komuro, T. Morikawa, and Y. Aoyagi, Local structure analysis of an optically active center in Er-doped ZnO thin film, J. Appl. Phys. 89 (2001) 3679–3684.

[7] L. Douglas, R. Mundle, R. Konda, C. E. Bonner, A. K. Pradhan, D. R. Sahu, and J.L. Huang, Influence of doping rate in Er^{3+}:ZnO films on emission characteristics, Opt. Lett. 33 (2008) 815–817.

[8] Z. Zhou, T. Komaki, A. Koizumi, T. Komori, M. Yoshino, M. Morinaga, Y. Fujiwara and Y. Takeda, Photoluminescence around 1.54 μm from Er-containing ZnO at Room Temperature, Mater. Trans. 45 (2004) 2003–2007.

[9] JCPDS card No 41−11506.

[10] JCPDS card No 36−1451.

[11] W.L. Dang, Y.Q. Fu, J.K. Luo, A.J. Flewitt, W.I. Milne, Deposition and characterization of sputtered ZnO films, Superlattices Microst. 42 (2007) 89–93.

[12] S.Y. Hua, Y.C. Lee, J.W. Lee, J.C. Huang, J.L. Shen, W. Water, The structural and optical properties of ZnO/Si thin films by RTA treatments, Appl. Surf. Sci. 254 (2008) 1578–1582.

[13] B. D. Ahn, S. H. Oh, C. H. Lee, G. H. Kim, H. J. Kim and S. Y. Leeb, Influence of thermal annealing ambient on Ga-doped ZnO thin films, J. Cryst. Growth 309 (2007) 128–133.

[14] H. Tong, Z. Deng, Z. Liu, C. Huang, J. Huang, H. Lan, C. Wang, Y. Cao, Effects of post-annealing on structural, optical and electrical properties of Al-doped ZnO thin films, Appl. Surf. Sci. 257 (2011) 4906–4911.

[15] B. L. Zhu, X. H. Sun, X. Z. Zhao, F. H. Su, G. H. Li, X. G. Wu, J. Wu, R. Wu and J. Liu, The effects of substrate temperature on the structure and properties of ZnO films prepared by pulsed laser deposition**,** Vacuum 82 (2008) 495–500.

[16] S. S. Lin, J. L. Huanga and P. Sajgalik, The properties of heavily Al-doped ZnO films before and after annealing in the different atmosphere, Surf. Coat. Technol. 185 (2004) 254–263.

[17] Y.X. Liu, Y.C. Liu, C.L. Shao, R. Mu, Excitonic properties of ZnO nanocrystalline films prepared by oxidation of zinc-implanted silica, J. Phys. D: Appl. Phys. 37 (2004) 3025–3029.

[18] S. A. Studenikin, M. Cocivera, W. Kellner, and H. Pascher, Band-edge photoluminescence in polycrystalline ZnO films at 1.7 K, J. Lumin. 91 (2000) 223.

[19] J. S. Kang, H. S. Kang, S. S. Pang, E. S. Shim, and S. Y. Lee, Investigation on the origin of green luminescence from laser-ablated ZnO thin films, Thin Solid Films. 443 (2003) 5−8.

[20] R. Va, M. J. Bushiri, and V. Vaidyan, Visible Luminescence Centers in Zinc Oxide Films Deposited by Spray Pyrolysis, J. Optoelectron Adv. M. 9 (2007) 3740.

[21] M. Liu, A. H. Kitai, and P. Mascher, Point defects and luminescence centres in zinc oxide and zinc oxide doped with manganese, J. Lumin. 54 (1992) 3542.

[22] Q. Luo, X. Qiao, X. Fan, and X. Zhang, Near-infrared emission of Yb^{3+} through energy transfer from ZnO to Yb^{3+} in glass ceramic containing ZnO nanocrystals, Opt. Lett. 36 (2011) 2767.

[23] X. L. Wu, G. G. Siu, C. L. Fu, and H. C. Ong, Photoluminescence and cathodoluminescence studies of stoichiometric and oxygen-deficient ZnO films, Appl. Phys. Lett. 78 (2001) 2285.

[24] B. J. Jin, S. Im and S.Y. Lee, Violet and UV luminescence emitted from ZnO thin films grown on sapphire by pulsed laser deposition, Thin Solid Films 366 (2000) 107−110.

[25] P. T. Hsieh, Y. C. Chen, M. S. Lee, K. S. Kao, M. C. Kao, M. P. Houng, The effects of oxygen concentration on ultraviolet luminescence of ZnO films by sol−gel technology and annealing, J. Sol-Gel Sci. Techn. 47 (2008) 1–6.

[26] C. Klingshirn, ZnO: From basics towards applications, Phys. Stat. Sol. (B) 244 (2007) 3027–3073.

[27] T. Nunokawa, O. Odawara H. Wada, Optical properties of highly crystalline Y_2O_3:Er,Yb nanoparticles prepared by laser ablation in water, Materials Research Express 1 (2014) 035043.

[28] W. G. van Sark, J. de Wild, J. Rath, A. Meijerink, R. Schropp, Upconversion in solar cells, Nanoscale Res Lett. 8 (2013) 881.

Figure captions

Fig. 1. Generic scheme of Er/Yb energy transfer; full vertical arrows represent the radiative decay, the dashed ones depict up-conversion processes and the curly lines indicate multi-phonon relaxation. Energy transfer processes are sketched by Yb-to-Er solid arrows. Russel-Saunders $^{2S+1}L_J$ notation was employed to refer to the f states: spin (S), orbital (L) and angular momentum (J) quantum numbers.

Fig. 2. X-ray diffraction patterns of as-deposited (AS DEP) ZnO:Er:Yb and that of films annealed in air (AIR),vacuum (VAC) and laser-annealed at three different laser powers (LAS1, LAS2, LAS3).

Fig. 3. Transmittance spectra for the as-deposited ZnO:Er:Yb films along with the air- and vacuum-annealed and the three laser-annealed ones. The inset table shows the integrated transmittance within the 400–800 nm wavelength range.

Fig. 4. Photoluminescence spectra, acquired at −196°C corresponding to the as-deposited ZnO:Er:Yb sample as well as the vacuum-, air- and laser-annealed ones, under 325 nm laser excitation. The inset displays PL emission peaks around 980 nm.

Fig. 5. Up-conversion PL spectra in logarithmic scale of the as-deposited sample, as well as the air-, the vacuum- and the three laser-annealed samples. 980 nm was selected as the excitation wavelength.

Table 1. Values of the *c*-parameter for the as-deposited, air annealed, vacuum annealed films and the films irradiated with three different laser powers.

Sample name	*c* (Å)
AS DEP	5.23 ± 0.02
AIR	5.20 ± 0.02
VAC	5.20 ± 0.02
LAS1	5.23 ± 0.02
LAS2	5.24 ± 0.02
LAS3	5.24 ± 0.02

Highlights

- Transparent and conducting ZnO:Er:Yb films were grown via magnetron sputtering.
- Post-annealing ZnO:Er:Yb is needed to optically activate Er ions.
- Visible up-conversion emission at 660 nm is observed under 980 nm excitation.
- A transparent and conducting up-converter is achieved by laser annealing.

Figure 1

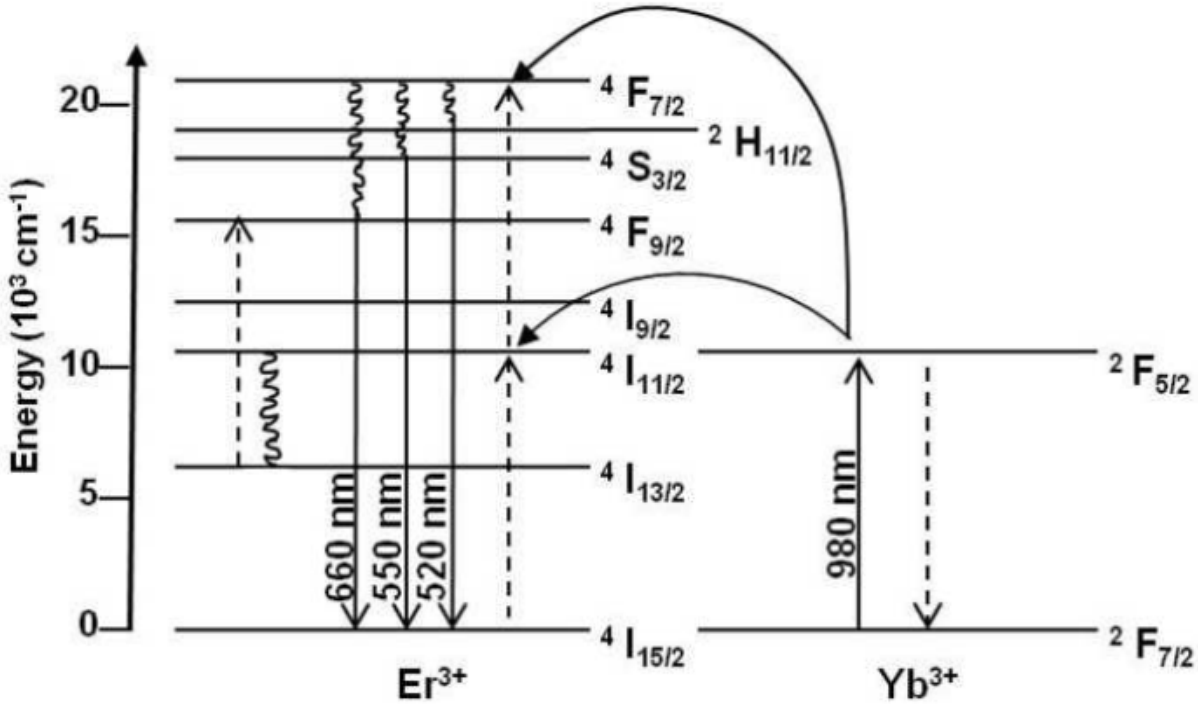
Energy (10^3 cm^{-1})
20
15
10
5
0
$^4F_{7/2}$
$^2H_{11/2}$
$^4S_{3/2}$
$^4F_{9/2}$
$^4I_{9/2}$
$^4I_{11/2}$
$^4I_{13/2}$
$^4I_{15/2}$
660 nm
550 nm
520 nm
Er^{3+}
980 nm
$^2F_{5/2}$
$^2F_{7/2}$
Yb^{3+}

Figure 2

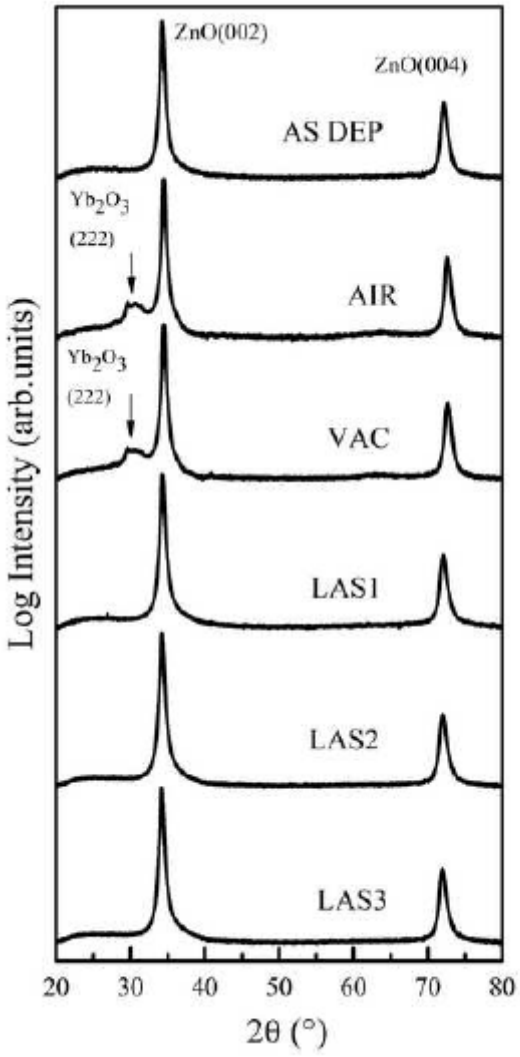
ZnO(002)
ZnO(004)
AS DEP
Yb2O3
(222)
AIR
Yb2O3
(222)
VAC
LAS1
LAS2
LAS3
Log Intensity (arb.units)
20
30
40
50
60
70
80
2θ (°)

Figure 3

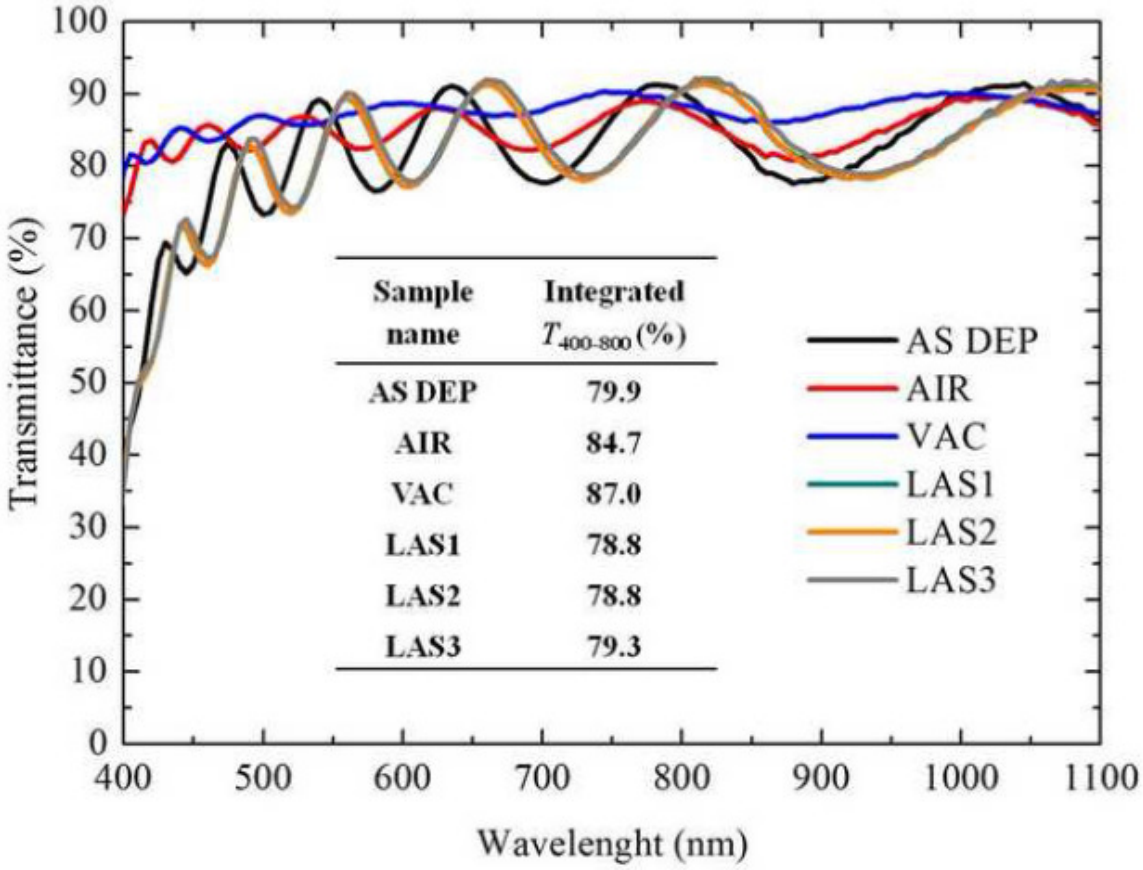

Sample name	Integrated $T_{400\text{-}800}$ (%)
AS DEP	79.9
AIR	84.7
VAC	87.0
LAS1	78.8
LAS2	78.8
LAS3	79.3

Figure 4

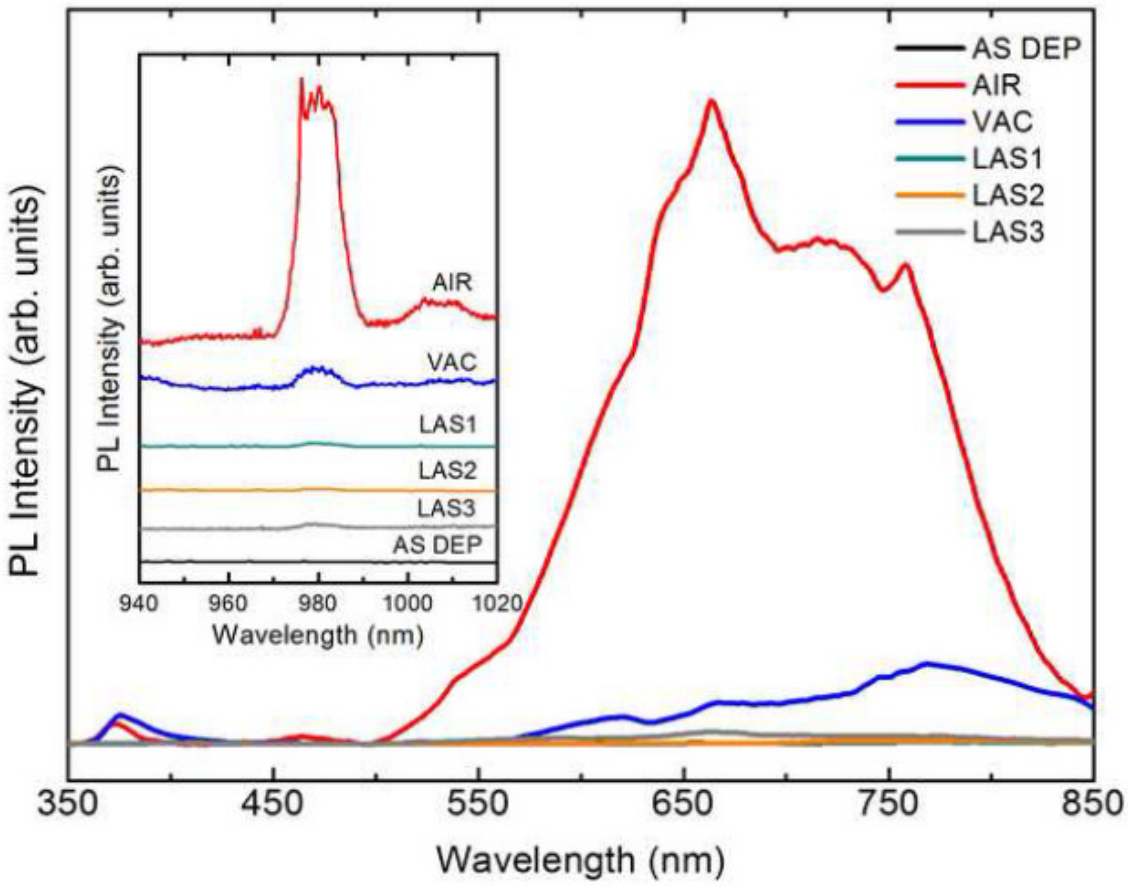
AS DEP
AIR
VAC
LAS1
LAS2
LAS3
PL Intensity (arb. units)
350
450
550
650
750
850
Wavelength (nm)
PL Intensity (arb. units)
AIR
VAC
LAS1
LAS2
LAS3
AS DEP
940
960
980
1000
1020
Wavelength (nm)

Figure 5

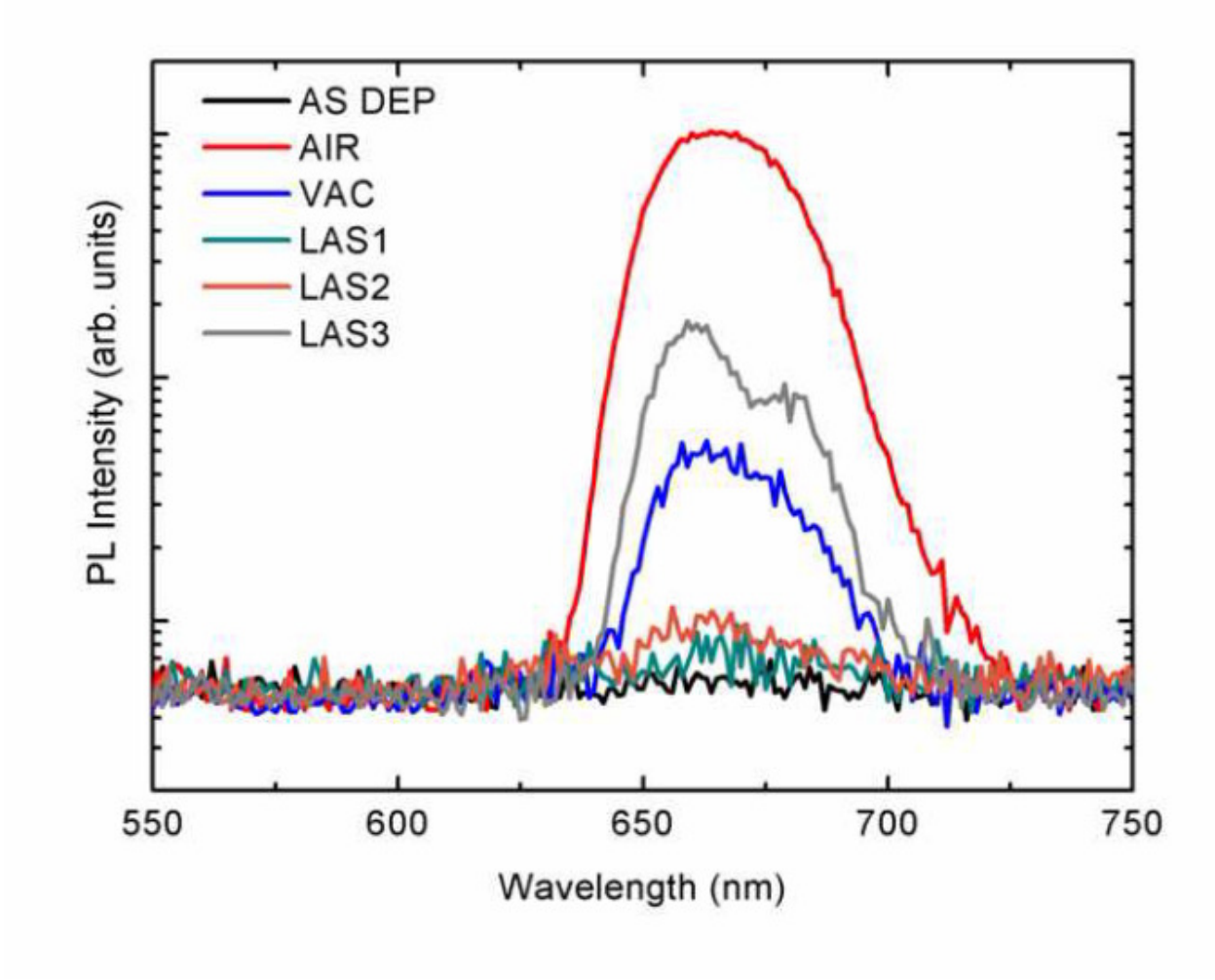
AS DEP
AIR
VAC
LAS1
LAS2
LAS3
PL Intensity (arb. units)
550
600
650
700
750
Wavelength (nm)